Flat plate boundary layer - Problem C1.3

Farshad Navah*, Brian Vermeire†, Siva Nadarajah‡

McGill University, Computational Aerodynamics Group

Case description

The problem aims at evaluating high-order solvers in computing the drag generated by airflow over a zero-thickness flat plate with a null angle of attack. The flow is laminar ($Re = 1 \cdot 10^6$), compressible ($Ma = 0.5$) and governed by the 2D Navier-Stokes equations, considering a ratio of specific heats of 1.4, a Prandtl number of 0.72 and constant dynamic viscosity.

Code description

The conservation laws are discretized by the correction procedure via reconstruction (CPR) scheme with DG correction functions [1]. The divergence of the inviscid fluxes are determined either through a chain rule or Lagrange polynomial approach. The Roe flux is employed as the common interface flux and the BR2 scheme for the viscous flux. As for boundary conditions, Riemann invariants are used in the far-field, while either slip or adiabatic non-slip on the walls. The dynamic viscosity coefficient is either held constant throughout the computational domain or obtained from the Sutherland's law. For the flat plate boundary layer case, the former is employed. Steady state solutions are obtained by using a Newton-Krylov algorithm, which serves as the primary solver. The sparse linear system of equations are solved using GMRES included in the PETSc package version *3.2-p7* along with the additive Schwarz method (ASM) as pre-conditioner. Before GMRES is employed, several block-Jacobi iterations are often performed. The solver is parallelized using MPI via Open MPI, version *1.4.3* where grid partitioning is achieved through ParMETIS. An implicit-explicit (IMEX) scheme [2] serves as a secondary solver, where a three-stage diagonally implicit Runge-Kutta (DIRK) is used. Each stage is split between an explicit and implicit sub-stage, where the non-stiff regions are solved with an explicit RK, while the stiff portions are solved through the above stated Newton approach. For the flat plate case, the IMEX solver was not employed. Post-processing is typically performed with Tecplot 360 and/or Gmsh version *2.8.5*.

Computations

The solution is initialized by freestream conditions. The L_2 norm of the x-momentum residuals is monitored to assess the convergence of the iterative solution by ensuring that the initial

*PhD Student, McGill University, Montreal, Quebec, Canada – farshad.navah@mail.mcgill.ca

†Post-Doctoral Scholar, Imperial College, London, United Kingdom

‡Associate Professor, McGill University, Montreal, Quebec, Canada

residuals are reduced by at least 10 orders of magnitude. The residuals are computed in the same way as suggested in the Third High-Order CFD Workshop guidelines.

The *Guillimin* cluster of the McGill high performance computing (MHPC) infrastructure, part of the Compute Canada and Calcul Québec HPC networks, served for the most intensive computations that used 4, 16 or 32 cores in parallel on two different architectures: sw and sw2/lm2. The rest of the calculations are performed on a quad-core personal computer (PC). Machine specifications and Taubench results are presented in Table 1.

Machine name	Specifications	Taubench CPU times (s)
MHPC-(sw)	Dual Intel Westmere EP Xeon X5650 (6-core, 2.66 GHz, 12MB Cache, 95W)	9.5
MHPC-(sw2/lm2)	Dual Intel Sandy Bridge EP E5-2670 (8-core, 2.6 GHz, 20MB Cache, 115W)	8.1
PC	Intel i7-4770 CPU (4-core, 3.40 GHz, 8MB Cache)	4.8

Table 1: Computer specifications

Meshes

A series of quad meshes is produced by removing every other line out of the *a5-125-2s.msh* mesh (provided by the First High-Order CFD Workshop), to which 5 levels of coarsening have been applied: from L-0 (original mesh) to L-4. As for the *a5-125-2s.msh*, the smallest elements are a pair of squares, symmetrical to the y axis and located at the leading-edge of the flat plate and the edge size growth ratio in each direction is found by considering a finite geometrical series. Table 2 provides the mesh characteristics.

Mesh	L-4	L-3	L-2	L-1	L-0 (a5-125-2s)
No. elements ($x \times y$)	28×20	56×40	112×80	224×160	448×320
No. elements on plate	18	36	72	144	288
Leading-edge spacing	45.2×10^{-5}	20.4×10^{-5}	9.72×10^{-5}	4.74×10^{-5}	2.34×10^{-5}
Off-wall spacing	45.1×10^{-5}	20.4×10^{-5}	9.72×10^{-5}	4.74×10^{-5}	2.34×10^{-5}

Table 2: Mesh characteristics

Sensitivity analysis

The sensitivity to the domain size is studied by taking the mesh *a3-125-2s.msh* (8,960 elements) of the First High-Order CFD Workshop as baseline. This mesh has the following

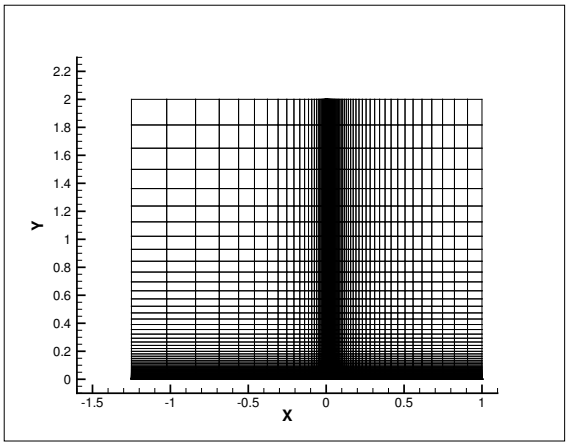

(a) original a3-125-2s.msh

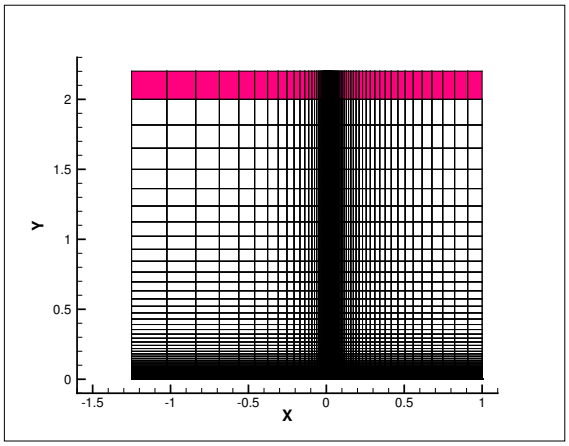

(b) extended by 1 layer on the top

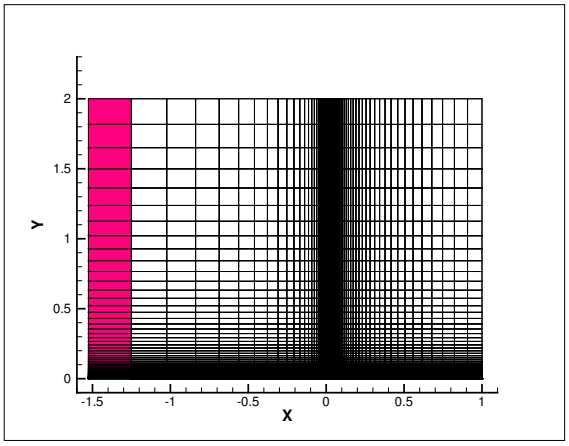

(c) extended by 1 layer on the left

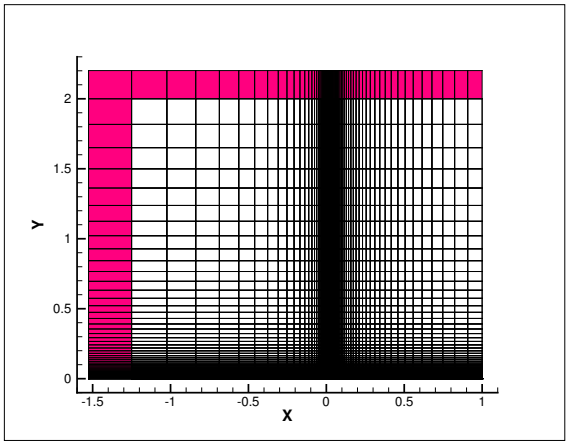

(d) extended by 2 layers

Figure 1: Domain size sensitivity analysis

domain size parameters: $L_H = 1.25$ and $L_V = 2$ which are respectively horizontal and vertical scales relative to the flat plate length. The drag solution is computed for the flow conditions described above and using a P4 polynomial discretization. The domain of the original mesh is extended once vertically, once horizontally and once in both directions simultaneously as illustrated in Figure 1. A layer of elements is added in each direction by respecting the original grid topology and cell size growth ratios. The added layers are coloured in magenta in Figure 1. The drag coefficient is recomputed in each case. The C_d results in Table 3 demonstrate that the domain described by the parameters $L_H = 1.25$ and $L_V = 2$, has a lesser influence on the drag than 0.01 of a count. This domain size is hence used for all of the computations.

L_H \ L_V	2.000	2.201
1.250	13.124×10^{-4}	13.122×10^{-4}
1.526	13.125×10^{-4}	13.123×10^{-4}

Table 3: Sensitivity of C_d to domain size parameters L_H and L_V

Results

The results for this case are presented in Tables 4 and 5 and Figures 3 and 4. Figure 2 shows the convergence of the x-momentum residuals for the L-2 grid and P1 to P5 solutions.

Consecutive p and h refinements are conducted until a minimal convergence of 10^{-6} in drag coefficient values is achieved (see Table 4). For C_d error computation, P5 solutions on meshes L-2 to L-0 are extrapolated by a Richardson formula [3] to yield the continuum solution estimate of $C_d = 1.31268 \times 10^{-3}$. The P5 solution on the L-0 grid was obtained by starting the computations from an interpolated P4 solution on the same grid. This solution is hence excluded from the work unit comparisons.

For P1 to P4, the plot of C_d error versus grid spacing in Figure 3 (a) shows converging values on the coarsest grids only, whereas the error increases as the grid is further refined. For P5, the asymptotic convergence is reached but the convergence rate is 1.2. These observations can be attributed to the presence of a singularity at the leading-edge of the flat plate. The local discretization error at the singularity evolves differently compared to the smooth flow regions. This negatively affects the monotonicity of the drag convergence and the precision of the continuum solution estimate via Richardson extrapolation.

To evaluate the impact of the singularity on the drag convergence, 0.35% of the flat plate length from the leading-edge is excluded from the drag computation. The reference value is recomputed in a similar fashion as for the full plate. The evolution of estimated errors versus mesh refinement is shown in Figure 3 (c). The error reduces with mesh refinement for all degrees of polynomial discretization. The corresponding convergence rates are computed by considering the two and three [3] finest solutions of each polynomial degree. The comparison

of 2-point versus 3-point convergence rates, presented in Table 5, reveals that the asymptotic convergence can only be assumed for P2, P4 and P5. However, only the convergence rate of P2 is in agreement with the theoretically expected value of 3.0. Improving the convergence of P3 to P5 solutions in a future work could be achieved by either decreasing the off-wall spacing or by starting the drag computation from a further point on the plate. A less heuristic approach would consist of controlling the discretization error via adaptation.

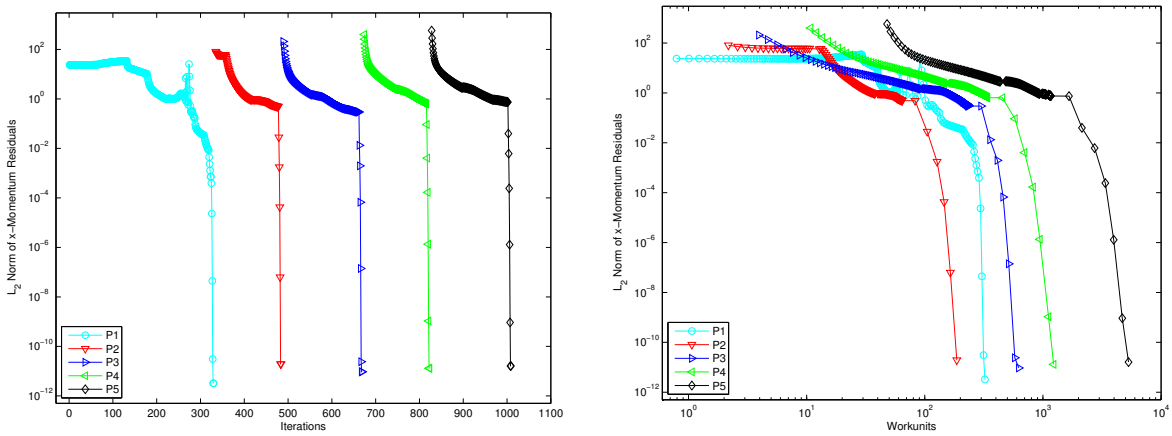

(a) Density residuals vs. iterations (b) Density residuals vs. work units

Figure 2: Iterative convergence

Polynomial degree	Mesh				
	L-4	L-3	L-2	L-1	L-0
P1	–	–	13.223×10^{-4}	13.126×10^{-4}	13.125×10^{-4}
P2	14.329×10^{-4}	13.374×10^{-4}	13.162×10^{-4}	13.126×10^{-4}	13.123×10^{-4}
P3	13.551×10^{-4}	13.170×10^{-4}	13.124×10^{-4}	13.123×10^{-4}	–
P4	13.857×10^{-4}	13.124×10^{-4}	13.124×10^{-4}	13.124×10^{-4}	–
P5	13.427×10^{-4}	13.123×10^{-4}	13.125×10^{-4}	13.126×10^{-4}	13.126×10^{-4}
P6	13.050×10^{-4}	–	–	–	–
P7	13.133×10^{-4}	–	–	–	–
P8	13.128×10^{-4}	–	–	–	–
P9	13.125×10^{-4}	–	–	–	–

Table 4: Drag coefficient (C_d) values; drag computed on full plate

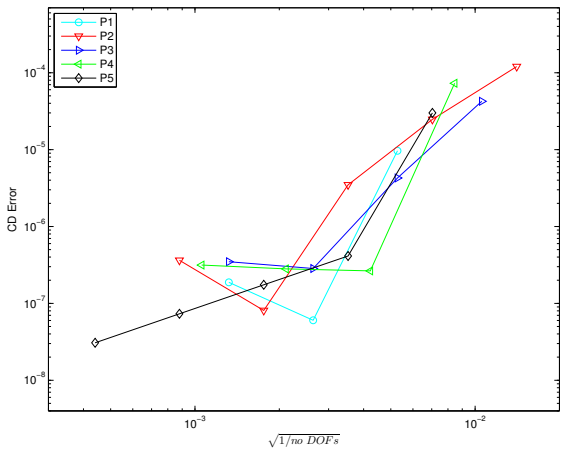

(a) C_d error (full plate) vs. h

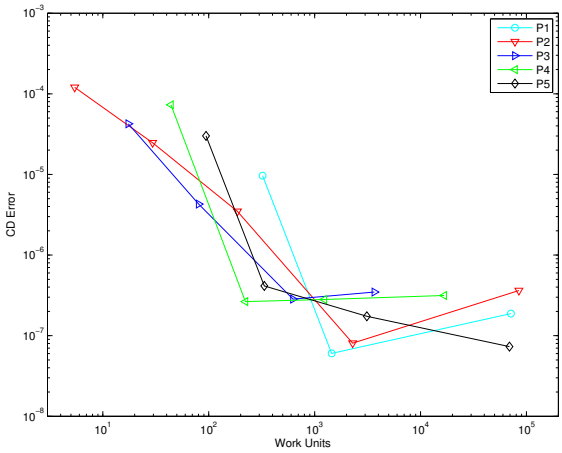

(b) C_d error (full plate) vs. work units

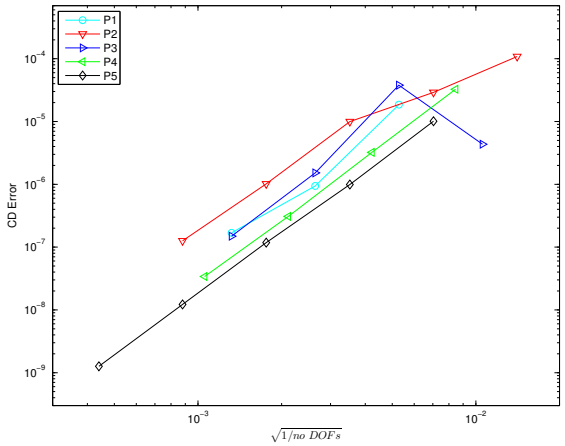

(c) C_d error ($0.0035 \leq x \leq 1$) vs. h

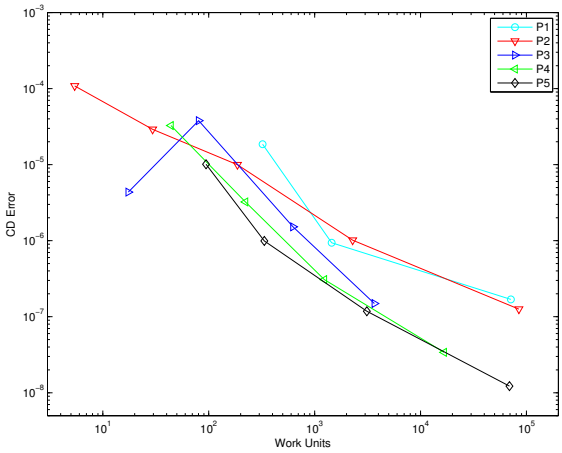

(d) C_d error ($0.0035 \leq x \leq 1$) vs. work units

Figure 3: C_d error results

polynomial degree	Convergence rates	
	3-points	2-points
P1	4.5	2.5
P2	3.3	3.0
P3	4.7	3.4
P4	3.4	3.2
P5	3.3	3.3

Table 5: Estimated rates of convergence to the continuum solution; drag computed on ($0.0035 \leq x \leq 1$)

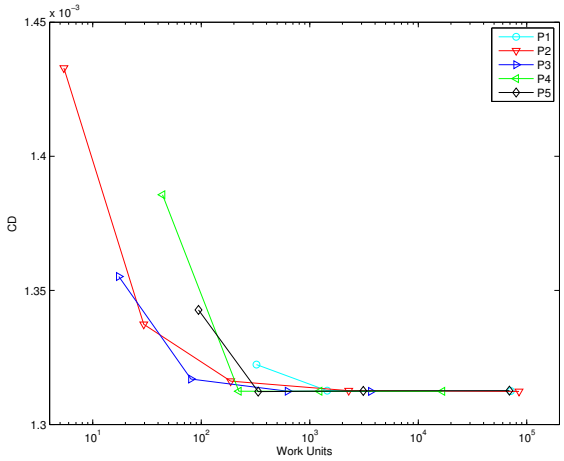

(a) C_d vs. work units - h-convergence

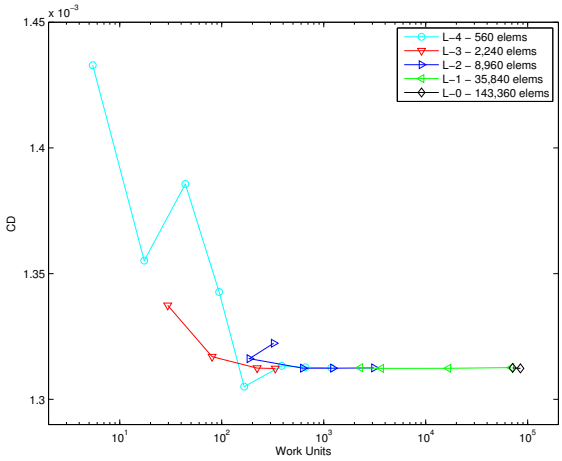

(b) C_d vs. work units - p-convergence

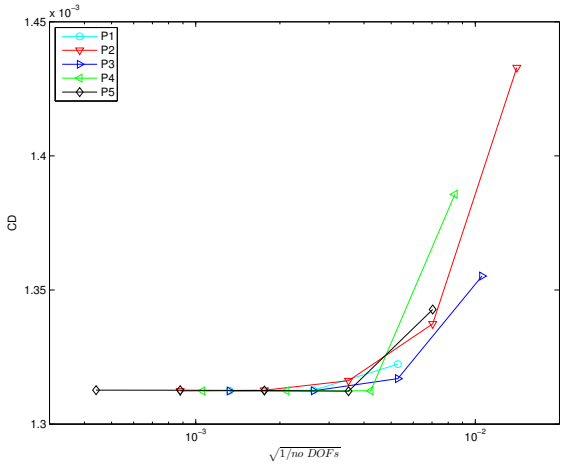

(c) C_d vs. h

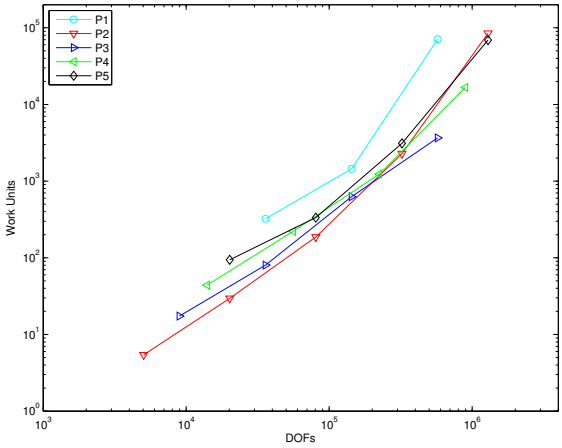

(d) Work units vs. DOFs

Figure 4: C_d results

References

[1] J. S. Cagnone, B. C. Vermeire, and S. Nadarajah. A p-adaptive LCP formulation for the compressible Navier-Stokes equations. *Journal of Computational Physics*, 233:pp. 324–338, 2013.

[2] B. C. Vermeire and S. Nadarajah. Adaptive IMEX schemes for high-order unstructured methods. *Journal of Computational Physics*, 280:261–286, January 2015.

[3] Examining Spatial (Grid) Convergence, http://www.grc.nasa.gov/WWW/wind/valid/tutorial/spatconv.html, accessed 2 September 2014.